# Modeling and Analysis of Vibration Characteristics of Rectangular Plate with Circular Through Hole Under Complex Boundary Conditions

*TANG Tianyi, HE Yijie, WU Jiajun, DONG Menglong, WANG Gang, NI Junfang**

School of Mechanical and Electrical Engineering, Soochow University, Suzhou 215131, P. R. China

(Received 13 March 2024; revised 3 June 2024; accepted 21 June 2024)

**Abstract:** This paper presents a method to study the free vibration of a plate with circular holes. The circular hole is regarded as a virtual small plate in which the mass density and Young's modulus are zero. Therefore, the free vibration problem of the circular hole plate can be transformed into the free vibration problem of the equivalent rectangular plate with non-uniform thickness. The model is derived from the spectral geometry method (SGM), and the displacement of the plate with circular holes is expanded by the modified Fourier series. Virtual springs are added to the boundary of the plate to simulate the boundary conditions of simply supported and fixed supports. The accuracy of this method is verified by comparison with the finite element calculation results. The relationship between modal numerical solutions of plates with circular holes and boundary conditions and geometry of the plate is studied.

**Key words:** round hole plate; spectral geometry method (SGM); energy method; virtual spring

**CLC number:** TB31 **Document code:** A **Article ID:** 1005-1120(2024)04-0515-11

## 0 Introduction

Perforated plate structures are widely used in various fields, such as aerospace, shipbuilding, and mechanical engineering. Compared with solid plates, perforated plates offer several advantages, such as high stiffness, low mass, and the ability to eliminate stress concentration, heat dissipation, and energy absorption. Rectangular plates with round through holes have a wide range of practical applications. In shipbuilding, perforated plates can be used for drainage and weight reduction; in engineering, they can provide space for the passage of cables, pipes or drive shafts, and in electronic equipment, they can be used for the entry and exit of electrical wires and for heat dissipation. The vibration characteristics of a perforated plate change after the introduction of perforations, and the analysis of these characteristics is crucial for the overall structural stability. There are several research methods for analyzing the vibration of perforated plates, including finite difference method, finite element method, boundary element method, differential quadrature method, Rayleigh-Ritz method, and domain decomposition method.

Research on the theory and engineering applications of perforated plates, both domestically and internationally, has achieved considerable results. Ali and Atwal[1] proposed a simplified method for dynamic analysis of perforated plates based on the Rayleigh principle. Lam et al.[2] introduced an exact numerical method for studying the vibration of perforated non-uniform rectangular plates based on the Rayleigh-Ritz method. Sabir and Davies[3] utilized the finite element method to investigate the natural frequencies and elastic buckling loads of square plates with reinforced square perforations under in-

*Corresponding author, E-mail address: jfni9999@sina.com.

**How to cite this article**: TANG Tianyi, HE Yijie, WU Jiajun, et al. Modeling and analysis of vibration characteristics of rectangular plate with circular through hole under complex boundary conditions[J]. Transactions of Nanjing University of Aeronautics and Astronautics, 2024, 41(4): 515-525.

http://dx.doi.org/10.16356/j.1005-1120.2024.04.008

plane loading. Wang et al.[4] improved the representation of displacement allowance functions for rectangular plates with openings using Fourier series. By combining displacement continuity conditions and the energy functional variational method, they obtained the natural frequencies of the perforated rectangular plates by variational optimization of unknown Fourier expansion coefficients to solve the standard eigenvalue equation. They also analyzed the effects of different boundary conditions, opening sizes, and opening positions on the free vibration characteristics of perforated plates. Wang et al.[5] studied the free vibration of rectangular plates with rectangular and triangular perforations within an equivalent geometric framework. Zhang et al.[6] extended the use of the Hencky bar network model (HBM) to analyze the vibration characteristics of rectangular plates with rectangular perforations. This model can compute the free vibration solutions of plates with various boundary conditions. Qiu et al.[7] employed a combined method of finite element and indirect boundary element to study the underwater vibration and acoustic radiation characteristics of steel plates with circular perforations, simply supported on four sides and without baffles. The studies showed that perforations can significantly alter the underwater vibration and acoustic radiation characteristics of the plates. Wang et al.[8] modeled an axisymmetric rotating nano circular plate and solved the governing differential equations of motion based on the Mindlin plate theory taking into account the nonlocal scaling and strain gradient effects using the differential product method. Abouelregal et al.[9] used the Laplace transform and Laplace inverse transform approximations to obtain solutions in field variables based on the Moore-Gibson-Thompson equations for a thermoelastic diffusion problem with cylindrical holes in an infinite medium. Civalek et al.[10-11] investigated the mechanical properties of cross-laminated composite plates reinforced with carbon nanotubes in terms of free vibration and buckling behavior by numerical solution using the first shear deformation theory and discrete singular convolution method, and investigated the natural frequency analysis of the sandwich beams with different configurations of S-shape function gradient, which was solved analytically by Navier's method for the case where the boundary conditions were simply supported. Zhang et al.[12] calculated the structural noise variation of rectangular concrete plates under different perforation conditions based on the low-frequency diffraction characteristics of box beam structures. The results indicated that after perforating the web, the total sound pressure level near the top plate, bottom plate, and web was reduced to different degrees in the frequency range of 1 Hz to 250 Hz, thereby controlling the structural noise of the box beam. Ni et al.[13-14] employed a Taylor series expansion and differential product method to establish the governing equations describing the nonlinear damped vibration of graphene nanosheet-reinforced composite dielectric membranes, and developed a two-step hybrid mechanical model to investigate the nonlinear damped vibration of functional gradient graphene nanosheet-reinforced composite dielectric membranes with internal pores. Qian et al.[15] investigated the nonlinear vibration characteristics of functional gradient graphene nanoplatelet-reinforced composite beams with Kelvin-Voigt damping using numerical methods. Yuan et al.[16] explored the free vibration characteristics of various perforated and reinforced plate models using the modified variational method, establishing a numerical tool suitable for dealing with complex plate structure problems. Zhong et al.[17] addressed the free vibration problem of functionally graded perforated parallelogram plates. Based on the first-order shear deformation laminated theory, they used isogeometric analysis (IGA) to investigate the vibration characteristics of functionally graded parallelogram plates with rectangular perforations. Pan[18] proposed a semi-analytical method for solving the plane stress distribution problem and the bending stress distribution problem of finite plates with arbitrary perforations. Based on this, they also presented a semi-analytical method for solving the stability problem of perforated plates and perforated stiffened plates. Mao et al.[19] utilized the complex potential method from anisotropic elasticity theory, employing Faber series and conformal mapping techniques to analyze the bending problem

of infinitely large anisotropic thin plates with multiple elliptical perforations. They obtained the series solution form for the bending of infinitely large anisotropic thin plates with multiple elliptical perforations.

The spectral geometry method (SGM) has garnered widespread attention and research in the academic domain. Kong et al.[20] focused on the acoustic-elastic plate coupling model, comparing and analyzing the effects of excitation position, cavity thickness, elastic boundary, and other factors on the acoustic radiation power, surface velocity, and cavity sound pressure of elastic plates under point force and point sound source excitations, as well as the differences between the two scenarios. Wang et al.[21-22] employed the SGM to establish displacement functions for Timoshenko beams with elastic constraints at the ends, proposing a unified approach to study Timoshenko beams with arbitrary variable cross-sections. Additionally, using the SGM, they represented the vibration displacement of rectangular plate structures with submerged elastic boundary constraints as Fourier cosine series with additional functions and investigated the acoustic radiation characteristics of submerged elastic boundary-constrained rectangular plates. Li et al.[23] investigated the free vibration of beams with material properties and arbitrary variations in cross-sections along the axial direction based on the SGM.

This paper treats the circular perforated portion of the plate as a virtual small plate with zero density and Young's modulus. Thus, the free vibration problem of perforated plates can be transformed into the free vibration problem of non-uniform thickness equivalent rectangular plates. By employing the SGM, the vibration displacement function of perforated plates is expanded using modified Fourier series, and the frequencies and mode shapes of the plate are obtained through the Rayleigh-Ritz method. A comparison between the obtained solutions and those simulated using finite element software is conducted to demonstrate the accuracy of this method. The paper discusses the effects of boundary conditions and perforation sizes on the natural frequencies, providing references for practical engineering applications.

## 1 Theoretical Analysis

Fig.1 illustrates a schematic diagram of an elastic constrained rectangular plate model with the circular through hole, where the openings are positioned arbitrarily on the plate. In the figure, $a$ and $b$ represent the length and width of the plate structure, respectively, and $R$ denotes the radius of the circular through hole. Elastic spring constraints, namely translational springs $k_a$ and torsional springs $K_a$, are applied to the four edges of the plate.

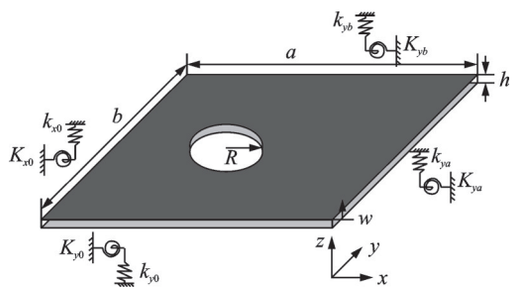


Fig.1 Model of a rectangular plate with circular through hole

Using Lagrange-Kirchhoff theory, the equation of the free vibration of the plate is

$$D\Delta^2 w(x,y)-\omega^2\rho w(x,y)=0 \quad \forall(x,y)\in S_p \tag{1}$$

where the plate displacement $w(x,y)$ is

$$W(x,y,t)=w(x,y)e^{i\omega t} \tag{2}$$

Considering that the circular hole portion of the plate is an extremely thin part of the plate, and its mass and Young's modulus are set to zero, the displacement function of the plate can be expressed as

$$\begin{aligned} w(x,y)=&\sum_{m=0}^{M}\sum_{n=0}^{N}A_{mn}\cos(\lambda_{am}x)\cos(\lambda_{bn}y)+\\ &\sum_{j=1}^{4}\left(\xi_b^j(y)\sum_{m=0}^{M}c_m^j\cos(\lambda_{am}x)+\right.\\ &\left.\xi_a^j(x)\sum_{n=0}^{N}d_n^j\cos(\lambda_{bn}y)\right) \end{aligned} \tag{3}$$

where

$$\xi_1(x)=\frac{9L}{4\pi}\sin\left(\frac{\pi x}{2L}\right)-\frac{L}{12\pi}\sin\left(\frac{3\pi x}{2L}\right) \tag{4}$$

$$\xi_2(x)=-\frac{9L}{4\pi}\cos\left(\frac{\pi x}{2L}\right)-\frac{L}{12\pi}\cos\left(\frac{3\pi x}{2L}\right) \tag{5}$$

$$\xi_3(x)=\frac{L^3}{\pi^3}\sin\left(\frac{\pi x}{2L}\right)-\frac{L^3}{3\pi^3}\sin\left(\frac{3\pi x}{2L}\right) \tag{6}$$

$$\xi_4(x)=-\frac{L^3}{\pi^3}\cos\left(\frac{\pi x}{2L}\right)-\frac{L^3}{3\pi^3}\cos\left(\frac{3\pi x}{2L}\right) \tag{7}$$

where $\lambda_{am}=m\pi/a$, $\lambda_{bn}=n\pi/b$, $A_{mn}$, $c_m^j$ and $d_n^j$ denote the unknown Fourier expansion coefficients to be determined, the auxiliary function functions $\xi_a^j(x)$ and $\xi_b^j(y)$ are introduced to overcome the discontinuities that may occur when the displacement function and its lower order derivatives are periodically extended to the whole $x$-$y$ plane for the calculation of arbitrary boundary conditions of the plate structure. The representations are shown in Eqs.(4—7). The superscript $j$ represents the serial number of the additional terms, and the subscripts $b$ and $a$ represent the values of $L$ in the corresponding expression.

The Lagrangian function of the plate structure can be expressed as

$$L_{\text{plate}}=U_{\text{plate}}-T_{\text{plate}} \tag{8}$$

where $U_{\text{plate}}$ is the total potential energy of transverse vibration of the plate and deformation of the restraining spring and $T_{\text{plate}}$ represents the total kinetic energy of the plate, which can be respectively expressed as

$$\begin{aligned}U_{\text{plate}}=&\frac{D}{2}\int_S\left\{\left(\frac{\partial^2 w}{\partial x^2}\right)^2+\left(\frac{\partial^2 w}{\partial y^2}\right)^2+\right.\\&\left.2\mu\frac{\partial^2 w}{\partial x^2}\frac{\partial^2 w}{\partial y^2}+2(1-\mu)\left(\frac{\partial^2 w}{\partial x\partial y}\right)^2\right\}\mathrm{d}S+\\&\frac{1}{2}\int_0^b\left[k_{x0}w^2+K_{x0}\left(\frac{\partial w}{\partial x}\right)^2\right]\Bigg|_{x=0}\mathrm{d}y+\\&\frac{1}{2}\int_0^b\left[k_{xa}w^2+K_{xa}\left(\frac{\partial w}{\partial x}\right)^2\right]\Bigg|_{x=a}\mathrm{d}y+\\&\frac{1}{2}\int_0^a\left[k_{y0}w^2+K_{y0}\left(\frac{\partial w}{\partial y}\right)^2\right]\Bigg|_{y=0}\mathrm{d}x+\\&\frac{1}{2}\int_0^a\left[k_{yb}w^2+K_{yb}\left(\frac{\partial w}{\partial y}\right)^2\right]\Bigg|_{y=b}\mathrm{d}x\end{aligned} \tag{9}$$

$$T_{\text{plate}}=\frac{\rho h\omega^2}{2}\int_S w^2\mathrm{d}S \tag{10}$$

where $S$ denotes the area of the plate, $D$ denotes the bending stiffness of the plate, $D=Eh^3/12(1-\mu^2)$, $\mu$ denotes the Poisson's ratio of the plate, and $\rho$ and $h$ denote the density and thickness of the plate, respectively. $k_{x0}$ and $K_{x0}$ are the stiffnesses of the translational and torsion springs located at $x=0$, respectively, and the stiffnesses of the remaining three sets of springs are also so defined. The Young's modulus and mass density at the hole location are

$$\begin{cases}E(x,y)=0\\ \rho(x,y)=0\end{cases}\quad(x,y)\in S_h \tag{11}$$

To simplify the integral calculations in Eqs.(9, 10), the perforated plate is gridded into small cells $S\times T$, as shown in Fig.2. The kinetic and potential energies of the cells whose geometric centers are located on the plate are calculated according to Eqs.(12, 13). Correspondingly, the kinetic and potential energies of the cells in the holes are omitted. By increasing the number of grids on the plate, the accuracy of the results can be increased. By using this numerical calculation method, the integrals in Eqs.(9, 10) will become

$$\begin{aligned}U_{\text{plate}}=&\frac{D}{2}\sum_{s=1}^{S}\sum_{t=1}^{T}P(s,t)R(s,t)+\\&\frac{1}{2}\int_0^b\left[k_{x0}w^2+K_{x0}\left(\frac{\partial w}{\partial x}\right)^2\right]\Bigg|_{x=0}\mathrm{d}y+\\&\frac{1}{2}\int_0^b\left[k_{xa}w^2+K_{xa}\left(\frac{\partial w}{\partial x}\right)^2\right]\Bigg|_{x=a}\mathrm{d}y+\\&\frac{1}{2}\int_0^a\left[k_{y0}w^2+K_{y0}\left(\frac{\partial w}{\partial y}\right)^2\right]\Bigg|_{y=0}\mathrm{d}x+\\&\frac{1}{2}\int_0^a\left[k_{yb}w^2+K_{yb}\left(\frac{\partial w}{\partial y}\right)^2\right]\Bigg|_{y=b}\mathrm{d}x\end{aligned} \tag{12}$$

$$T_{\text{plate}}=\frac{\rho h\omega^2}{2}\sum_{s=1}^{S}\sum_{t=1}^{T}H(s,t)R(s,t) \tag{13}$$

where $S$ and $T$ are the number of cells along the $x$ and $y$ directions, and $P(s,t)$ and $H(s,t)$ are the potential and kinetic energies of the $(s,t)$ cells, respectively. $R(s,t)=1$ if the geometric center of the $(s,t)$ element is located on the plate, otherwise, $R(s,t)=0$.

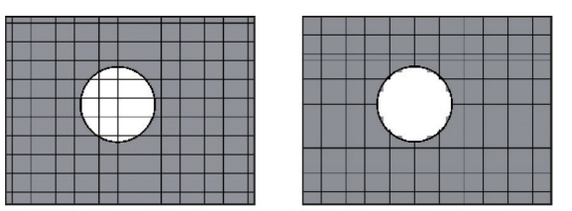

(a) Meshing of the plate (b) Meshing of the plate with hole

Fig.2 Meshing of the rectangular plate containing circular through hole

Assuming that a simple harmonic point force of amplitude $F$ is applied to the face of the perforated plate and the point of action is $(x_0, y_0)$, the work $W_F$ done by this force can be expressed as

$$W_F = \iint_S Fw\delta(x - x_0)\delta(y - y_0)\mathrm{d}x\mathrm{d}y \quad (14)$$

where $\delta$ is the Dirac function.

By substituting Eqs.(12—14) into the Lagrangian generalized Eq.(8) for the plate and applying variational differentiation to the coefficients, the equations of control for free and forced vibration of the open plate structure are obtained shown as

$$\left\{\left[\boldsymbol{K}_{\mathrm{p\_h}}\right] - \omega^2\left[\boldsymbol{M}_{\mathrm{p\_h}}\right]\right\}\{\boldsymbol{A}\} = \{\boldsymbol{F}\} \quad (15)$$

where $\boldsymbol{K}_{\mathrm{p\_h}}$, $\boldsymbol{M}_{\mathrm{p\_h}}$, $\boldsymbol{A}$ and $\boldsymbol{F}$ denote the stiffness matrix, the mass matrix, the Fourier coefficient matrix and the force matrix of the perforated plate, respectively, and the free and forced vibration behaviors of the perforated plate with circular holes can be obtained by solving this system of equations.

## 2 Convergence and Validation

The theoretical model of the plate with circular holes is constructed in the previous section, and the convergence and accuracy of the method used in this paper need to be verified next. The dimensions of the rectangular plate are set to be $a \times b = 0.5\ \mathrm{m} \times 0.6\ \mathrm{m}$, thickness $h = 0.001\ \mathrm{m}$, density $\rho = 2\ 770\ \mathrm{kg/m^3}$, Young's modulus $E = 71\ \mathrm{GPa}$, Poisson's ratio $\upsilon = 0.33$, and the centroid of the circular hole is set to be (0.2 m, 0.3 m) with radius $R = 0.1\ \mathrm{m}$.

The face of the thin plate is set as a free boundary, and constraint springs are applied to the four sides of the plate to simulate arbitrary boundary conditions. The boundary springs consist of a continuous translational, which restricts the translational motion of the plate in the $z$-direction and a torsional spring which restricts the rotational motion of the plate about the $z$-axis. The following validation examples use the three classical boundary conditions of simple, fixed, and free, where the simple boundary condition can be realized by setting the translational spring stiffness to infinity and the torsion spring stiffness to zero, and the fixed boundary condition can be realized by setting both the translational spring stiffness and the torsion spring stiffness to infinity. For the free boundary condition, both translational and rotational stiffnesses are set to zero. The boundary conditions of the four sides of the plate are set to be free boundary (FFFF), simply supported boundary (SSSS) and solidly supported boundary (CCCC), and the number of meshes $S \times T = 80 \times 80$. Table 1 demonstrates the first nine orders of the intrinsic frequencies of the plate with cir-

**Table 1 The first nine order natural frequencies of plates with circular holes obtained by two methods** Hz

| | Modal order | 1 | 2 | 3 | 4 | 5 | 6 | 7 | 8 | 9 |
|---|---|---|---|---|---|---|---|---|---|---|
| FFFF | $M=N=2$ | 9.940 | 13.074 | 21.161 | 26.362 | 29.612 | 43.110 | 53.675 | 53.869 | 61.759 |
| | $M=N=4$ | 9.896 | 12.884 | 20.534 | 26.194 | 29.547 | 41.681 | 51.334 | 53.358 | 59.250 |
| | $M=N=6$ | 9.884 | 12.778 | 20.184 | 26.003 | 29.457 | 40.958 | 51.225 | 52.736 | 58.235 |
| | $M=N=8$ | 9.881 | 12.748 | 20.061 | 25.873 | 29.385 | 39.737 | 51.059 | 52.210 | 57.700 |
| | $M=N=10$ | 9.879 | 12.742 | 20.029 | 25.805 | 29.334 | 38.819 | 50.929 | 51.908 | 57.427 |
| | $M=N=12$ | 9.878 | 12.741 | 20.023 | 25.787 | 29.311 | 38.432 | 50.853 | 51.832 | 57.316 |
| | $M=N=14$ | 9.877 | 12.741 | 20.021 | 25.784 | 29.302 | 38.320 | 50.827 | 51.821 | 57.284 |
| | $M=N=16$ | 9.876 | 12.740 | 20.020 | 25.784 | 29.299 | 38.291 | 50.819 | 51.818 | 57.277 |
| | $M=N=18$ | 9.876 | 12.740 | 20.019 | 25.783 | 29.297 | 38.284 | 50.817 | 51.816 | 57.275 |
| | $M=N=20$ | 9.876 | 12.740 | 20.018 | 25.782 | 29.296 | 38.282 | 50.816 | 51.814 | 57.272 |
| | FEM | 9.863 | 12.735 | 20.008 | 25.752 | 29.267 | 38.241 | 50.757 | 51.733 | 57.226 |
| SSSS | $M=N=20$ | 16.384 | 33.513 | 42.660 | 62.028 | 73.662 | 90.216 | 105.294 | 109.153 | 112.701 |
| | FEM | 16.363 | 33.464 | 42.583 | 61.940 | 73.626 | 90.052 | 105.230 | 109.030 | 112.690 |
| CCCC | $M=N=20$ | 33.814 | 50.159 | 68.386 | 85.306 | 102.402 | 123.490 | 140.289 | 140.771 | 144.400 |
| | FEM | 33.923 | 50.310 | 68.625 | 85.559 | 102.801 | 123.760 | 140.820 | 141.420 | 145.021 |

cular holes computed by the present method and finite element method (FEM). The finite element method is modeled and calculated using ANSYS software with shell181 cells, and the grid cell size is set to 0.005 m.

As can be seen from Table 1, with the gradual increase of the truncation number $M=N$, the intrinsic frequency of the plate with circular holes under the free boundary gradually converges, and the modal solution values obtained by the present method basically coincide with the results of the finite element calculations when $M=N=20$, proving that the convergence of the present method is reliable. Figs. 3 and 4 show the 1st, 3rd, 5th, 7th and 9th order modal shapes of the plate with circular holes obtained by the present method under both free and solidly supported boundary conditions, respectively, and compare with those obtained by ANSYS. It can be seen that the vibration patterns obtained by the two methods are very consistent, which verifies the accuracy of the present method in predicting the free vibration of the perforated plate.

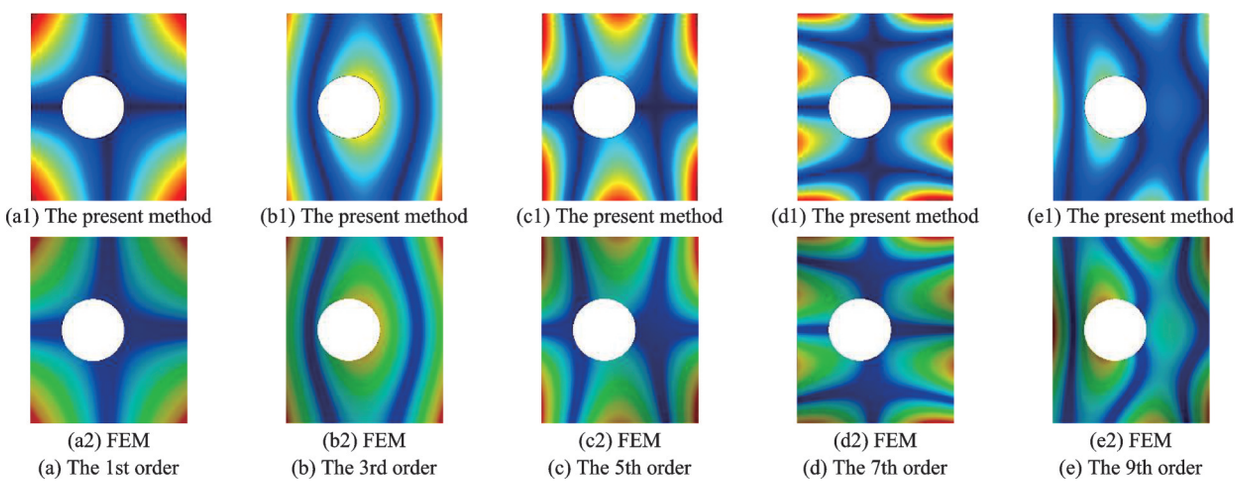


Fig.3 Comparison of modal shapes of free boundary plate obtained by the present method and FEM

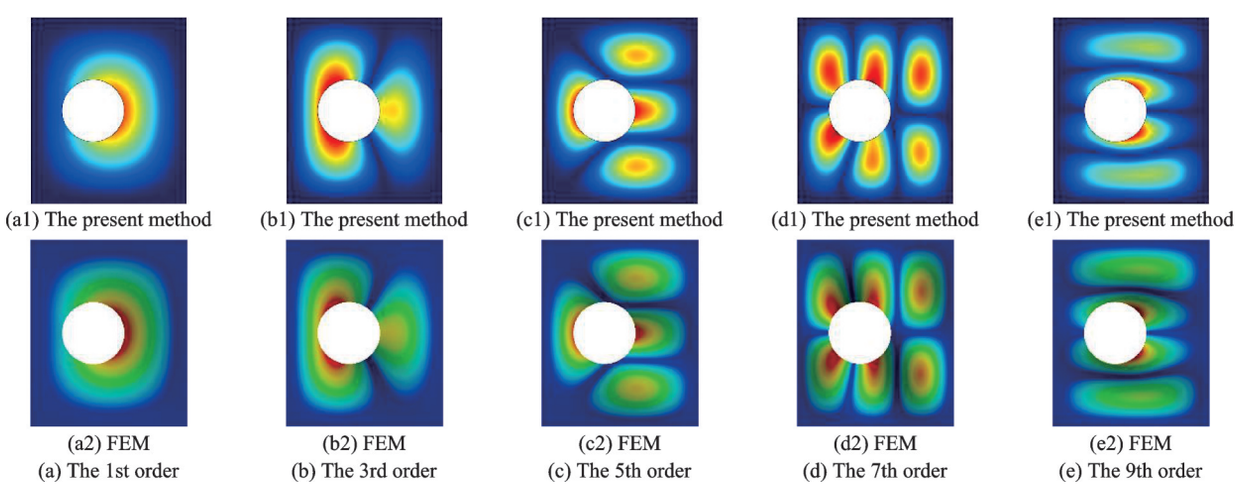


Fig.4 Comparison of modal shapes of clamped boundary plate obtained by the present method and FEM

Fig.5 shows the comparison between the amplitude-frequency response at (0.3 m, 0.1 m) on the perforated plate and the excitation point selected at (0.4 m, 0.5 m) on the plate. The amplitude of the excitation force is 100 N, the direction is along the $z$-axis, and the boundary conditions are SSSS and CCCC, respectively. It can be found that the amplitude-frequency response of the plate obtained by the present method is very much in line with that obtained by the finite element method.

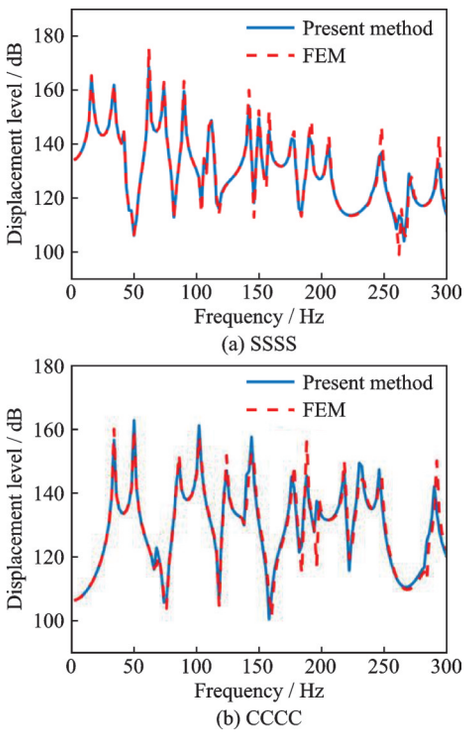


Fig.5 Comparison of amplitude-frequency response at (0.3 m, 0.1 m) on the plate containing circular through hole

## 3 Results and Discussion

In engineering applications, the boundary conditions for the installation of planar thin plates, the size of the through holes, and the thickness of the plates all have an impact on the vibration behavior of the plates. The validation part of Section 2 yields the intrinsic frequencies and vibration patterns of the plate with circular holes under three classical boundary conditions. In this section, the choice of boundary conditions is enriched with the addition of three boundary conditions, FFSS, FFCC, and SSCC, and the geometrical and material parameters of the plate with circular holes used in the previous section are adopted. Fig.6 demonstrates the first six orders of the intrinsic frequencies of the plate under the five boundary conditions.

As can be seen in Fig.6, the overall trend of the intrinsic frequency of the plate increases during the change of boundary conditions from FFSS to CCCC. This is due to the fact that the increase in the stiffness and number of constrained springs leads to a larger overall stiffness value of the plate, which

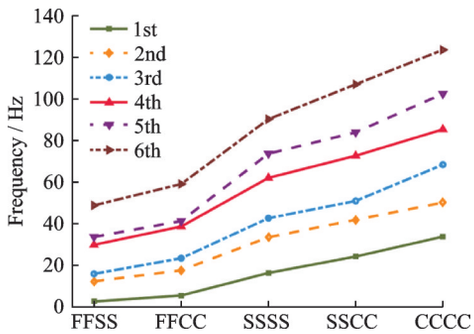


Fig.6 The first six order natural frequencies of plate containing circular through hole with different boundaries

results in an increase in the intrinsic frequency. The most pronounced upward trend in boundary conditions is from FFCC to SSSS. This is because the effect of linear spring stiffness on the intrinsic frequency is greater than the effect of torsional spring stiffness on the intrinsic frequency. Among the five boundary conditions, the plate has the highest intrinsic frequency for the CCCC boundary condition and the lowest intrinsic frequency for the FFSS boundary condition.

Next, to compare the effect of the size of the open circular hole on the vibration characteristics of the plate, the geometrical and material parameters of the plate with the circular hole used in the previous section are still used, and the radius of the open circular hole is varied to observe the change in the intrinsic frequency of the plate. Fig.7 demonstrates the comparison of the first six orders of intrinsic frequencies of the flat plate with circular hole radii of 0 m (no openings), 0.05 m, 0.1 m, and 0.15 m for the four boundary conditions of FFSS, SSSS, SSCC, and CCCC, respectively. From the results in the figure, it can be seen that the first six orders of the intrinsic frequency of the plate under the FFSS boundary all decrease with the increase of the radius of the open circular hole, whereas there is no obvious pattern of the effect of the radius of the open circular hole on the intrinsic frequency of the plate under the other four boundary conditions. Observing the fundamental frequency of the plate, it is found that there is a significant jump in the fundamental frequency increase when the radius of the cir-

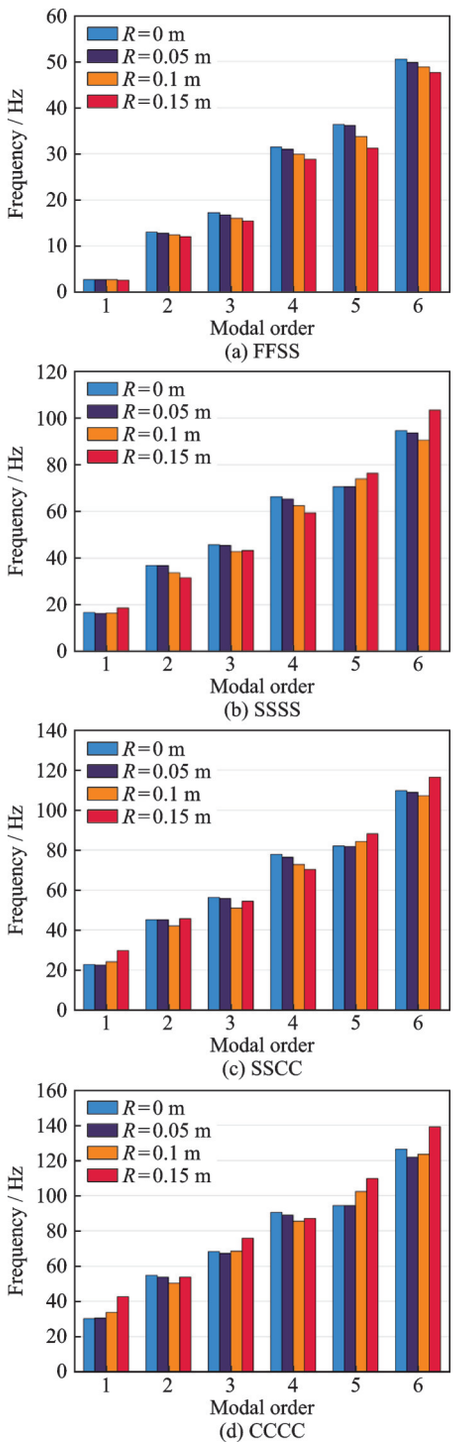


Fig.7 Variation of the first six orders of natural frequencies of plate containing circular through hole as a function of the radius of the circular hole

cular hole is varied from 0.1 m to 0.15 m under the SSSS, SSCC and CCCC boundaries. The reason is that when the radius of the circular hole is changed from 0.1 m to 0.15 m, the mass of the plate decreases dramatically compared with the previous one, but the stiffness of the plate does not decrease significantly due to the simple or solid support of the four edges, so the intrinsic frequency has increased significantly.

The previous parametric analyses are carried out under some classical boundary conditions. In practical engineering, the plate boundary installation conditions are often complex, not limited to classical boundaries such as solid support and simple support, but more often elastic boundary support occurs. The first four orders of the intrinsic frequency of the perforated plate with respect to the stiffness of the translational and torsional springs are given in Fig.8. In order to make the analysis more intuitive, the springs are first dimensionless, $k_a^3/D$ represents the stiffness of the translational springs, while $K_a/D$ represents the stiffness of the torsion springs, and the spring stiffnesses of the four boundaries of the plate are equal. From the figure, it can be seen that the intrinsic frequency of the plate gradually increases and eventually stabilizes at one value as the linear and torsion spring stiffnesses increase. The improvement of the intrinsic frequency of the plate structure by the translational spring stiffness is more pronounced compared with the limited improvement of

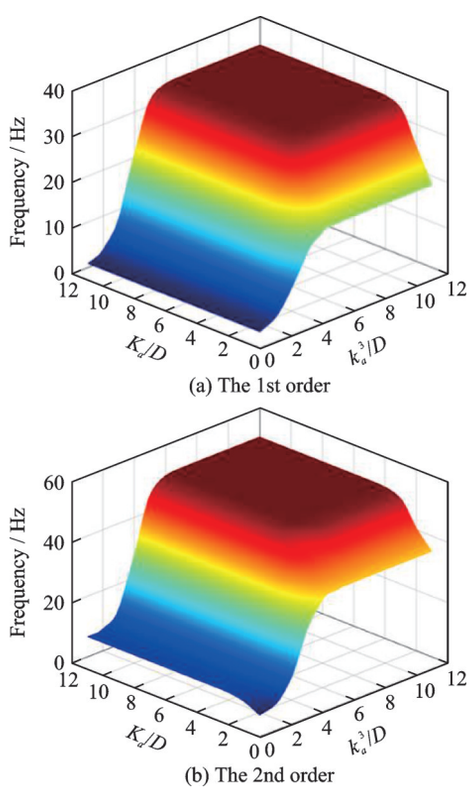

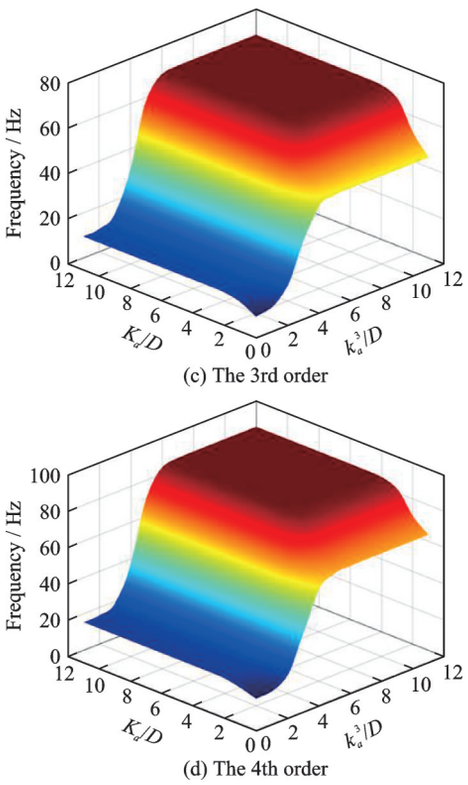


Fig.8 Variation of natural frequencies of plate containing circular through hole as a function of the stiffness of linear and torsion springs

the intrinsic frequency of the plate structure by the torsional spring stiffness. The intrinsic frequency results of the plate stabilize when the linear spring stiffness $k_a^3/D > 7$, and similarly when the torsion spring stiffness $k_a^3/D > 4$.

The results in Fig.9 demonstrate the effect of plate thickness $h$ on the amplitude frequency response of the perforated plate at (0.3 m, 0.1 m) for different boundaries. From the figure, it can be noticed that the first resonant frequency of the amplitude frequency response of the plate increases as the plate thickness increases, which is due to the fact that the increase in plate thickness enhances the fundamental frequency of the perforated plate. It is not difficult to find that the first resonant frequency of the amplitude-frequency response of the plate is linearly related to the change in plate thickness. It can also be seen from the figure that the amplitude of the response displacement decreases with the increase of the plate thickness, which indicates that increasing the plate thickness can effectively suppress the vibration behavior of the perforated plate.

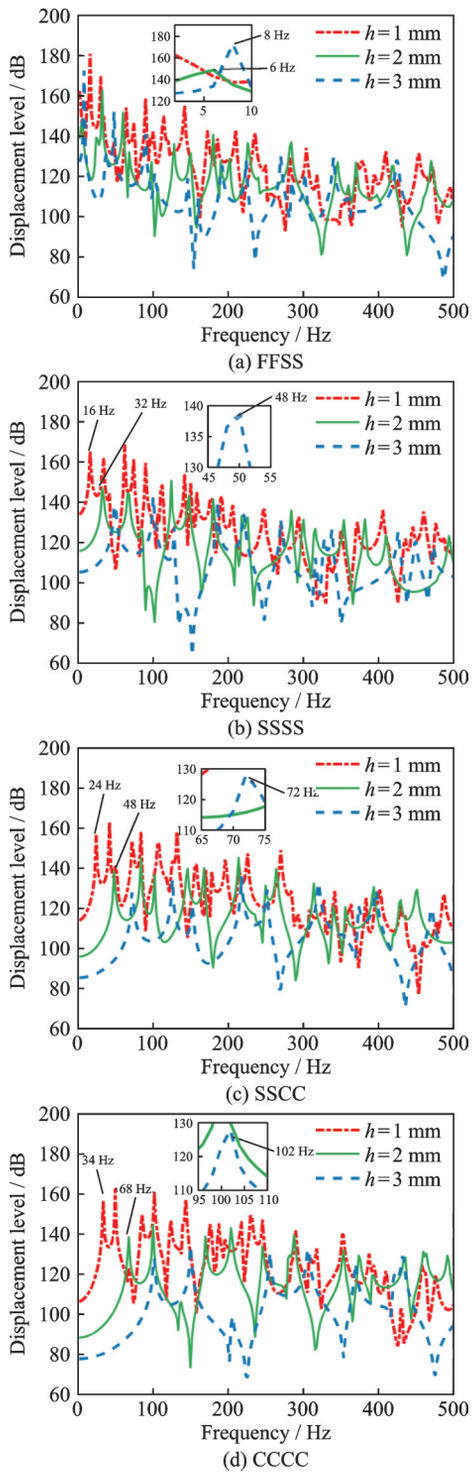


Fig.9 Effect of plate thickness $h$ on the amplitude-frequency response at (0.3 m, 0.1 m) for plate containing circular through hole with different boundaries

## 4 Conclusions

The spectral geometry method is used to study the vibration of an elastically restrained plate with circular holes, the displacement of the plate with circular holes is expressed using a modified Fourier series expansion, an auxiliary function is introduced to

overcome the discontinuities that may occur when the displacement function and its lower-order derivatives are periodically extended to the whole $x$-$y$ plane, the vibration modes of the plate with circular holes are solved by the Rayleigh-Ritz method, and the accuracy of the present method is verified by comparing with results obtained by simulation with finite-element software ANSYS. The effect of boundary condition and circular hole size on the intrinsic frequency is discussed. The study introduces an analytical approach that offers significant engineering value by accurately predicting the vibration characteristics of plates with circular holes across diverse boundary conditions. Notably, the proposed method in the paper is distinguished by its low-dimensional vibration control equation set, which ensures rapid convergence, high computational efficiency, and maintains sufficient accuracy, thereby establishing it as a reliable tool for engineering applications. The following conclusions are obtained:

(1) The first six orders of the intrinsic frequency of the plate all decrease with the increase of the radius of the open circular hole at the FFSS boundary, and there is a significant jump in the fundamental frequency increase when the radius of the circular hole is varied from 0.1 m to 0.15 m at the SSSS, SSCC, and CCCC boundaries.

(2) As the linear and torsion spring stiffnesses are increased, the intrinsic frequency of the plate gradually increases and eventually stabilizes at one value. The results of the intrinsic frequency of the plate tend to stabilize when the linear spring stiffness $k_a^3/D > 7$ and when the torsion spring stiffness $k_a^3/D > 4$.

(3) The first resonant frequency of the amplitude-frequency response of the plate increases as the plate thickness increases. The first resonant frequency of the amplitude-frequency response of the plate is linearly related to the change of the plate thickness, and the amplitude of the response displacement decreases with the increase of the plate thickness, which indicates that the increase of the plate thickness can effectively suppress the vibration behavior of the perforated plate.

## References

[1] ALI R, ATWAL S J. Prediction of natural frequencies of vibration of rectangular plates with rectangular cutouts[J]. Computers & Structures, 1980, 12(6): 819-823.

[2] LAM K Y, HUNG K C, CHOW S T. Vibration analysis of plates with cutouts by the modified Rayleigh-Ritz method[J]. Applied Acoustics, 1989, 28(1): 49-60.

[3] SABIR A B, DAVIES G T. Natural frequencies of square plates with reinforced central holes subjected to inplane loads[J]. Thin-Walled Structures, 1997, 28(3/4): 337-353.

[4] WANG Minhao, LI Kai, QIU Yongkang, et al. Free vibration characteristics analysis of rectangular plate with rectangular opening based on Fourier series method[J]. Chinese Journal of Ship Research, 2017, 12(4): 102-109. (in Chinese)

[5] WANG G, LI W L, FENG Z H, et al. A unified approach for predicting the free vibration of an elastically restrained plate with arbitrary holes[J]. International Journal of Mechanical Sciences, 2019, 159: 266-277.

[6] ZHANG Y P, WANG C M, PEDROSO D M, et al. Extension of Hencky bar-net model for vibration analysis of rectangular plates with rectangular cutouts[J]. Journal of Sound and Vibration, 2018, 432: 65-87.

[7] QIU C L, CHEN Z G, DENG Y, et al. Underwater vibration and acoustic radiation characterization of open plates[J]. Chinese Journal of Ship Research, 2013, 8(6): 75-80.

[8] WANG X Y, LUO Q Y, LI C, et al. On the out-of-plane vibration of rotating circular nanoplates[J]. Transactions of Nanjing University of Aeronautics and Astronautics, 2022, 39(1): 23-35.

[9] ABOUELREGAL A E, ERSOY H, CIVALEK Ö. Solution of Moore-Gibson-Thompson equation of an unbounded medium with a cylindrical hole[J]. Mathematics, 2021, 9(13): 1536.

[10] CIVALEK Ö, DASTJERDI S, AKGÖZ B. Buckling and free vibrations of CNT-reinforced cross-ply laminated composite plates[J]. Mechanics Based Design of Structures and Machines, 2022, 50(6): 1914-1931.

[11] AVCAR M, HADJI L, CIVALEK Ö. Natural frequency analysis of Sigmoid functionally graded sandwich beams in the framework of high order shear deformation theory[J]. Composite Structures, 2021, 276: 114564.

[12] ZHANG Tianqi, LUO Yanyun, ZHOU Li. Effect of web hole on vibration and noise of rail transit box girder[J]. Journal of Traffic and Transportation Engineering, 2019, 19(4): 35-46. (in Chinese)

[13] NI Z, FAN Y, HANG Z, et al. Damped vibration analysis of graphene nanoplatelet reinforced dielectric membrane using Taylor series expansion and differen-

tial quadrature methods[J]. Thin-Walled Structures, 2023, 184: 110493.
[14] NI Z, FAN Y, HANG Z, et al. Numerical investigation on nonlinear vibration of FG-GNPRC dielectric membrane with internal pores[J]. Engineering Structures, 2023, 284: 115928.
[15] QIAN Q, ZHU F, FAN Y, et al. Parametric study on nonlinear vibration of FG-GNPRC dielectric beam with Kelvin-Voigt damping[J]. Thin-Walled Structures,2023,185: 110617.
[16] YUAN Guoqing, YU Yu, WANG Zonglong, et al. Free vibration analysis on structures of plates with hole reinforcement plates based on modified variational method[J]. Computer Aided Engineering, 2017, 26(2): 58-64. (in Chinese)
[17] ZHONG Rui, HU Shuang, QIN Bin, et al. Isogeometric vibration analysis of functionally graded perforated parallelogram plates with holes[J]. Journal of Harbin Engineering University, 2022, 43(7): 999-1005. (in Chinese)
[18] PAN Zuxing. Semi-analytical methods for stress and stability analyses of perforated plates[D]. Wuhan: Huazhong University of Science and Technology, 2014. (in Chinese)
[19] MAO Chunjian, XU Xiwu, GUO Shuxiang. Stress analysis of anisotropic infinite thin plate with multiple elliptical holes[J]. Engineering Mechanics, 2012, 29(9): 80-86. (in Chinese)
[20] KONG Deyu, WANG Gang, NI Junfang. Acoustic radiation characteristics of cavity-elastic plate model under different excitation[J]. Journal of Mechanical Engineering, 2021, 57(21): 126-137. (in Chinese)
[21] WANG G, LI W, LIU T S. The average radiation efficiency of a plate immersed in water with general boundary conditions[J]. Mechanics Research Communication, 2020, 106: 103532.
[22] WANG G, LI W L, LI W Y, et al. A unified procedure for the vibration analysis of elastically restrained Timoshenko beams with variable cross sections[J]. Noise Control Engineering Journal, 2020, 68(1): 38-47.
[23] LI G F, WANG G, NI J F, et al. The vibration analysis of the elastically restrained functionally graded Timoshenko beam with arbitrary cross sections[J]. Journal of Low Frequency Noise, Vibration and Active Control, 2021. DOI: 10.1177/14613484211019648.

**Acknowledgements** This work was supported by the National Natural Science Foundation of China (No.51805341) and the Science and Technology Major Project of Ningbo City (No.2021Z098).

**Authors** Mr. **TANG Tianyi** received the B.S. degree from School of Mechanical and Electrical Engineering, Soochow University in 2023, and is currently pursuing MA. Eng in School of Mechanical and Electrical Engineering, Soochow University. Main research interests are in mechanical engineering, vibration and mechanics, etc.

Prof. **NI Junfang** received the M.S. degree from Harbin Institute of Technology in 1995, and Ph.D. degree Shanghai Jiaotong University in 1998. His research interests include CNC and manufacturing technology.

**Author contributions** Mr. **TANG Tianyi** completed the calculation of data results and simulation comparison, and wrote the third and fourth parts of the manuscript. Mr. **HE Yijie** integrated the theoretical model and completed the first and second parts of the manuscript. Mr. **WU Jiajun** refined and reviewed the third and fourth parts of the manuscript. Mr. **DONG Menglong** refined and reviewed the first and second parts of the manuscript. Prof. **WANG Gang** provided the project, designed the study, and complied the models. Prof. **NI Junfang** provided funding and reviewed the manuscript. All authors commented on the manuscript draft and approved the submission.

**Competing interests** The authors declare no competing interests.

(Production Editor: XU Chengting)

# 复杂边界条件下含圆形通孔的矩形板振动特性建模及分析

唐天逸，何逸杰，吴佳俊，董梦龙，王　刚，倪俊芳

(苏州大学机电工程学院,苏州 215131,中国)

**摘要**:提出了一种研究带圆孔弹性约束平板自由振动的方法。该方法将圆孔视为一个虚拟小板,其密度和杨氏模量为零,则带圆孔板的自由振动问题可以转化为非均匀厚度等效矩形板的自由振动问题。该模型基于谱几何法(Spectral geometry method, SGM)导出,用修正的傅里叶级数展开带圆孔板的位移;在板的边界加入虚拟弹簧以模拟板的简支和固支边界条件。通过与有限元计算结果的对比,验证了该方法的准确性。同时本文还研究了带圆孔板模态数值解与边界条件和板的几何尺寸的关系。

**关键词**:圆孔板;谱几何法;能量法;虚拟弹簧